Phase Difference Control of Single-Phase Grid Forming Inverters for Fault Detection

Grant T. McKechnie and Alejandro D. Domínguez-García

Department of Electrical and Computer Engineering
University of Illinois Urbana-Champaign
Email: {granttm2, aledan}@illinois.edu

***Abstract*—This paper presents a strategy for controlling the phase differences of a three-phase voltage source made up of single-phase droop-controlled grid forming inverters arranged in a delta configuration. We derive a linear model approximately describing the system phase dynamics, and use it to formulate a Linear Quadratic Integral (LQI) controller capable of phase angle reference tracking. The proposed controller enables the system to be operated as a three-phase balanced source. Unbalanced operation is also desirable when supplying an unbalanced load or injecting auxiliary signals. MATLAB simulations are used to validate the proposed controller and demonstrate performance under nominal and unbalanced conditions. The LQI controller ensures minimal overshoot, zero steady-state error, and robust reference tracking in both the linearized and nonlinear model used to derive it. The results exemplify the flexibility of the controller tuning for precise shaping of system response, which is essential for adapting inverter-based resources (IBRs) to grid protection requirements.**

***Index Terms*—Grid forming (GFM) inverters, phase difference control, Delta connection, droop control, linear quadratic integral (LQI) control**

I. Introduction

Grid forming (GFM) inverters are emerging as a way to facilitate the integration of renewable energy resources by providing virtual inertia and enabling both frequency and voltage control. However, GFM inverters are limited by their minimal fault current contribution of 1.2-2.0 per unit (see [1]), which is constrained by current-limiting mechanisms designed to protect sensitive switching electronics. Legacy protection schemes are calibrated for synchronous generators, which can reliably deliver five to ten times the rated current for short durations during faults without damaging components [2]. During faults, IBRs behave like current sources that limit large currents and keep the negative sequence current close to zero, even during faults [3]. This can cause relay malfunction because of inaccurate estimation of fault impedances [4] [5].

In this paper, we show how control of single-phase GFM inverters arranged in a delta configuration can be leveraged to create unbalanced sources for the purpose of injecting auxiliary signals for fault detection and identification, an idea that has been explored in [6]. The controller is able to intentionally cause voltage unbalance which leads to the generation of negative sequence currents. We derive the angular dynamics of the proposed system, demonstrate the design of a LQI controller for phase angle control around the phase-balanced equilibrium, and evaluate the closed-loop time-domain behavior. By regulating phase angles, the system can act as an unbalanced three-phase source to facilitate fault identification in a network. The controller also helps the system maintain balanced three-phase operation during normal conditions.

This work was supported in part by the U.S. Department of Energy's Office of Energy Efficiency and Renewable Energy (EERE) through Solar Energy Technologies Office (SETO), under Grant 38637 (UNIFI consortium), and by the U.S. National Science Foundation under Award Number 2411926.

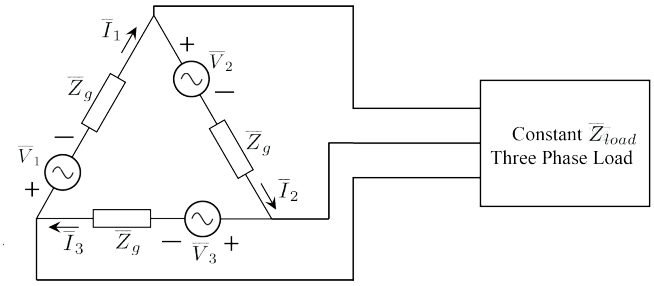

Fig. 1. Equivalent-circuit model of three delta-connected single-phase inverters in phasor domain serving a generic constant impedance three-phase load

II. System Model

The system considered comprises three single-phase delta-connected GFM inverters supplying a balanced three-phase constant impedance load; see Fig. 1 for the equivalent-circuit model representation. The load may be either wye- or delta-connected. The system features the following elements:

1) A digital phase-locked loop (PLL) which is used to track voltage angles at the output of each inverter.
2) Active and reactive power sensors, which are used at the output of each inverter
3) A central controller, which receives all phase angles and power measurements and performs the pertinent calculations for controlling all three inverters.

The objective of this paper is to design a closed-loop control strategy for regulating the inverter phase differences to some desired values.

A. Individual Inverter Model

The phenomena of interest are slow enough so that the dynamics of the inner control loops, which are much faster, can

be ignored (see [7] for justification). The model of each GFM inverter can therefore be reduced to a controllable voltage source behind an impedance as shown in Fig. 1. Let R_g and L_g respectively denote the series resistance and inductance of the grid side of the inverter LCL filter, and define $X_g = \omega^\circ L_g$, where ω° is the nominal frequency of the inverter. The phasor associated with the voltage across the LCL-filter capacitive branch of the ℓ^{th} inverter is

$$\overline{V_\ell} = V_\ell \angle \theta_\ell, \quad \ell = 1, 2, 3, \tag{1}$$

where V_ℓ denotes the voltage rms magnitude, and θ_ℓ denotes the time integral of the inverter frequency ω_ℓ. In a similar way, let $\overline{I_\ell}$ denote the phasor associated with the current across the impedance $\overline{Z}_g = R_g + jX_g$.

Each inverter has a droop controller that generates a reference voltage waveform. The inner current control loop is much faster than the outer voltage control loop. Therefore, we assume that the voltage generated behind the reactance perfectly matches the reference waveform. Due to the single-phase nature of the inverters, a 120 Hz harmonic oscillation exists in the generated power waveforms. In practice, power measurements are filtered to eliminate this harmonic component [8]; however, for analysis purposes, we assume perfect elimination. Let P_ℓ and Q_ℓ respectively denote the filtered measurements of the ℓ^{th} inverter active and reactive power output. Let $P_\ell^\star(t)$ and $Q_\ell^\star(t)$ respectively denote the active and reactive power setpoints of the ℓ^{th} inverter; these references will be generated from an external LQI controller which will be discussed later. Then, the amplitude and frequency for the ℓ^{th} single-phase inverter are given by

$$V_\ell = V^\circ - m_q(Q_\ell - Q_\ell^\star(t)), \tag{2}$$

$$\dot{\theta}_\ell = \omega^\circ - m_p(P_\ell - P_\ell^\star(t)), \tag{3}$$

where V° is the nominal voltage, and where we select the droop slopes, m_q and m_p, to have a 5% voltage deviation and a 0.5-Hz frequency swing, as complex power changes across the range of rated power, S_r. Thus,

$$m_q = 0.05\frac{V^\circ}{S_r}, \quad m_p = \frac{2\pi \cdot 0.5}{S_r}. \tag{4}$$

B. Nonlinear Model Formulation

For the system under consideration (see Fig.1), assume the following hold:

A1. The power absorbed by the inverter filters' impedance is negligible

A2. Reactive power droop has a negligible effect on phase dynamics (see [9] for a detailed derivation of this assumption).

A3. When $u_\ell = 0$, $\ell = 1, 2, 3$, the steady-state power generation of each inverter matches the corresponding per-phase active power load, which we denote by $P_{\ell,load}$. This quantity is assumed to be constant, close to the rated power, and known apriori.

A4. Control is applied to the $P_\ell^*(t)$ signal additively, i.e.,

$$P_\ell^*(t) = P_{\ell,load} + u_\ell(t).$$

Under Assumptions A1 — A4, it can be shown (see [9]) that the total real power delivered by each inverter is

$$P_\ell = \sum_{k=1}^{3} \frac{(V^\circ)^2}{|\overline{Z}_{loop}|} \cos(\theta_k(t) - \theta_\ell(t) - \phi) + P_{\ell,load}, \tag{5}$$

where

$$|\overline{Z}_{loop}| = \sqrt{(3R_g)^2 + (3X_g)^2}, \quad \phi = \tan^{-1}(\frac{X_g}{R_g}). \tag{6}$$

Substituting (5) into (3) yields the following phase dynamics

$$\dot{\theta}_\ell(t) = \omega^\circ - K\sum_{k=1}^{3} \cos(\theta_k(t) - \theta_\ell(t) - \phi) + m_p u_\ell(t), \tag{7}$$

where

$$K = \frac{m_p(V^\circ)^2}{|\overline{Z}_{loop}|}. \tag{8}$$

C. Coordinate Transformation

From here on, we write any time-varying signal $x(t)$ as x for notational convenience. For control design purposes, it is convenient to write the phase dynamics in (7) of two of the inverters relative to the phase dynamics of the third one. Without loss of generality, choose the dynamics of inverter #1 as the reference and define

$$\theta_{21} = \theta_2 - \theta_1, \quad \theta_{31} = \theta_3 - \theta_1,$$
$$u_{21} = u_2 - u_1, \quad u_{31} = u_3 - u_1.$$

Assume that control effort to inverter #1 is equal to zero for all time, thus $u_{21} = u_2$ and $u_{31} = u_3$. After trigonometric and algebraic manipulations of (7), the dynamics of the phase differences are described by:

$$\frac{d}{dt}\begin{bmatrix}\theta_{21}\\ \theta_{31}\end{bmatrix} = \begin{bmatrix} f_1(\theta_{21}, \theta_{31}, u_2)\\ f_2(\theta_{21}, \theta_{31}, u_3)\end{bmatrix}, \tag{9}$$

where

$$f_1 = K\Big[2\sin\theta_{21} + \sin\theta_{31} + \sin(\theta_{21} - \theta_{31})\Big]\sin\phi \tag{10}$$
$$+ K\Big[\cos\theta_{31} - \cos(\theta_{21} - \theta_{31})\Big]\cos\phi + m_p u_2,$$
$$f_2 = K\Big[2\sin\theta_{31} + \sin\theta_{21} + \sin(\theta_{31} - \theta_{21})\Big]\sin\phi \tag{11}$$
$$+ K\Big[\cos\theta_{21} - \cos(\theta_{31} - \theta_{21})\Big]\cos\phi + m_p u_3.$$

The equilibrium points of (9) are obtained by setting $\dot{\theta}_{21} = \dot{\theta}_{31} = 0, u_2 = u_3 = 0$, and solving for θ_{21} and θ_{31}. While six equilibrium points exist within $[0, 2\pi)$ as shown in [9], we only focus on one of the phase-balanced equilibria which is asymptotically stable

$$\bar{\theta}_{21} = \frac{4\pi}{3}, \ \bar{\theta}_{31} = \frac{2\pi}{3}. \tag{12}$$

D. Linearization and Stability Analysis of Equilibrium point

To design our controller, we will rely on a linearized model of the system around the phase-balanced equilibrium point. Define small phase and control perturbations from the phase-balanced equilibrium as follows:

$$\delta\theta_{21} = \theta_{21} - \bar{\theta}_{21}, \quad \delta\theta_{31} = \theta_{31} - \bar{\theta}_{31},$$
$$\delta u_2 = u_2 - \bar{u}_2, \quad \delta u_3 = u_3 - \bar{u}_3.$$

The Jacobian matrix for the phase differences as

$$\mathbf{J}(\theta_{21}, \theta_{31}) = \begin{bmatrix} \frac{\partial f_1}{\partial \theta_{21}} & \frac{\partial f_1}{\partial \theta_{31}} \\ \frac{\partial f_2}{\partial \theta_{21}} & \frac{\partial f_2}{\partial \theta_{31}} \end{bmatrix}, \tag{13}$$

and by setting $\theta_{21} = \bar{\theta}_{21} = \frac{4\pi}{3}$ and $\theta_{31} = \bar{\theta}_{31} = \frac{2\pi}{3}$, we obtain

$$\mathbf{J}(\bar{\theta}_{21}, \bar{\theta}_{31}) = K \begin{bmatrix} -\frac{3}{2}\sin\phi + \frac{\sqrt{3}}{2}\cos\phi & -\sqrt{3}\cos\phi \\ \sqrt{3}\cos\phi & -\frac{3}{2}\sin\phi - \frac{\sqrt{3}}{2}\cos\phi \end{bmatrix}. \tag{14}$$

The off diagonal terms represent the cross coupling between the states. Note that coupling between states is maximized when $\phi = 0$ (resistive Δ-loop) and approaches 0 as $\phi \to \frac{\pi}{2}$ (primarily inductive Δ-loop). The linearized system around the phase-balanced equilibrium is then given by

$$\frac{d}{dt}\begin{bmatrix} \delta\theta_{21} \\ \delta\theta_{31} \end{bmatrix} = \mathbf{J}(\bar{\theta}_{21}, \bar{\theta}_{31}) \begin{bmatrix} \delta\theta_{21} \\ \delta\theta_{31} \end{bmatrix} + \begin{bmatrix} m_p & 0 \\ 0 & m_p \end{bmatrix} \begin{bmatrix} u_2 \\ u_3 \end{bmatrix}. \tag{15}$$

The eigenvalues of the matrix (14) are

$$\lambda_{1,2} = -\frac{3}{2}K(\sin(\phi) \pm j\cos\phi), \tag{16}$$

both of which have strictly negative real parts when $\phi \in (0, \frac{\pi}{2}]$; this means that the phase-balanced equilibrium is locally stable in the absence of control.

III. Controller Design

The primary objective of the controller design is to regulate the phase angle differences to their desired reference values. While a variety of control strategies can be employed to achieve this goal, we selected the LQI controller for its robust performance and time-domain response shaping capabilities.

LQI controllers minimize a cost function that balances control effort and system performance. While this approach introduces additional complexity compared to traditional methods, especially in tuning and selecting weighting matrices, it offers significant advantages in transient-response specifications. Careful adjustment of these matrices allows precise shaping of the closed-loop time-domain response for each state and control input. Moreover, LQI controllers are well-suited for multiple-input multiple-output (MIMO) systems, where strong coupling between the dynamics of individual states may exist. In contrast, conventional proportional-integral (PI) controllers may struggle to manage complex interactions which are inherent to MIMO systems, potentially leading to unstable behavior.

By leveraging the strengths of the LQI framework, we can effectively coordinate control actions across all states, ensuring stability and desired transient performance. The process to design a LQI controller for a nonlinear system starts with analyzing the dynamics of the linearized system around an equilibrium point. A controller is formulated for the linearized system and then adapted for the nonlinear system.

A. Background

Define $\delta\theta = \begin{bmatrix} \delta\theta_{21}, & \delta\theta_{31} \end{bmatrix}^\top$, $u = \begin{bmatrix} u_2, & u_3 \end{bmatrix}^\top$, and $y = \delta\theta$. The linearized phase angle dynamics in (15) can be rewritten as follows

$$\frac{d}{dt}\delta\theta = A\delta\theta + Bu, \tag{17}$$
$$y = C\delta\theta, \tag{18}$$

where

$$A = \mathbf{J}(\bar{\theta}_{21}, \bar{\theta}_{31}), \tag{19}$$
$$B = \begin{bmatrix} m_p & 0 \\ 0 & m_p \end{bmatrix}, \tag{20}$$
$$C = \begin{bmatrix} 1 & 0 \\ 0 & 1 \end{bmatrix}. \tag{21}$$

In order for y to track a reference signal r with minimal steady state error, we will develop a LQI controller. The first step to design such a robust controller requires the introduction of integral states, which we denote by q. These integral states will serve to regulate the integral of the difference between the reference signal

$$r = \begin{bmatrix} \delta\theta_{21}^r \\ \delta\theta_{31}^r \end{bmatrix}, \tag{22}$$

and y to zero; i.e.,

$$\dot{q} = r - C\delta\theta := e.$$

Because y keeps track of two states, $\delta\theta_{21}$ and $\delta\theta_{31}$, we will need two integral states. Writing the reference signal and integral states out explicitly, we obtain

$$\frac{d}{dt}q = \frac{d}{dt}\begin{bmatrix} q_1 \\ q_2 \end{bmatrix} = \frac{d}{dt}\begin{bmatrix} \delta\theta_{21}^r - \delta\theta_{21} \\ \delta\theta_{31}^r - \delta\theta_{31} \end{bmatrix} \tag{23}$$

Define $z = \begin{bmatrix} \delta\theta^\top, & q^\top \end{bmatrix}^\top$; then the augmented system can be written in state space-form as

$$\dot{z} = \underbrace{\begin{bmatrix} A & 0 \\ -C & 0 \end{bmatrix}}_{A_z} z + \underbrace{\begin{bmatrix} B \\ 0 \end{bmatrix}}_{B_z} u + \underbrace{\begin{bmatrix} 0 \\ I \end{bmatrix}}_{B_r} r. \tag{24}$$

$$y = \underbrace{\begin{bmatrix} C & 0 \end{bmatrix}}_{C_z} z. \tag{25}$$

To design the controller, we need to solve the optimal control problem stipulated by the following cost function applied to the augmented system

$$J = \int_0^\infty \left(z^\top \underbrace{\begin{bmatrix} Q_\theta & 0 \\ 0 & Q_i \end{bmatrix}}_{Q_z} z + u^\top R u \right) dt, \tag{26}$$

where $Q_\theta \in \mathbb{R}^2$, which is positive definite, is designed to penalize large states, $Q_i \in \mathbb{R}^2$, which is positive definite, penalizes integral errors, and $R \in \mathbb{R}^2$, which is positive definite, penalizes control actuation. The control u that minimizes (26) is of the form

$$u = -R^{-1}B_z^\top P_z z, \tag{27}$$

where P_z is a solution to the following augmented Algebraic Riccati Equation (ARE):

$$P_z A_z + A_z^\top P_z - P_z B_z R^{-1} B_z^\top P_z + Q_z = 0. \tag{28}$$

B. LQI Existence Conditions and Synthesis

For there to exist a unique positive definite stabilizing solution P_z to the augmented ARE, the following conditions must hold [10]

i. $R \succ 0$ and $Q_z \succeq 0$,
ii. (A_z, B_z) is stabilizable
iii. $(A_z, Q_z^{1/2})$ is detectable

In order to simplify the design, let Q_θ, Q_i and R be diagonal matrices defined as

$$Q_\theta = \text{diag}(a_1, a_2), \tag{29}$$
$$Q_i = \text{diag}(b_1, b_2), \tag{30}$$
$$R = \text{diag}(r_1, r_2), \tag{31}$$

where $a_1, a_2, b_1, b_2, r_1, r_2 > 0$ ensures that all weighting matrices are positive definite and thus requirement (i) is fulfilled.

The augmented system is stabilizable if all eigenvalues of A_z with non-negative real parts are controllable. We apply the Popov-Belevitch-Hautus (PBH) test for stabilizability. First we compute the eigenvalues of A_z. For each unstable eigenvalue, we must verify that the rank of the matrix $M = [\lambda I - A_z \mid B_z]$ is equal to the rank of the augmented system [11]. The augmented system state matrix, A_z, has two unstable eigenvalues at 0. We must apply the PBH test to ensure that these unstable modes are controllable to validate the stabilizability of the augmented system. Let us construct the M matrix for these unstable eigenvalues as follows

$$M = \begin{bmatrix} 0 \cdot I - A & 0 & B \\ C & 0 \cdot I - 0 & 0 \end{bmatrix}.$$

The rank of this matrix is equal to the rank of

$$M' = \begin{bmatrix} -A & B \\ C & 0 \end{bmatrix}.$$

Because rank(M') = 4 = rank(A_z), the PBH test confirms that the augmented system is stabilizable, thus fulfilling requirement (ii).

For the pair $(A_z, Q_z^{1/2})$ to be detectable, all the unstable eigenmodes of A_z must be observable through $Q_z^{1/2}$. To prove this, let

$$Y = \begin{bmatrix} \lambda I - A_z \\ Q_z^{1/2} \end{bmatrix}. \tag{32}$$

The pair $(A_z, Q_z^{1/2})$ is detectable if

$$\text{rank}(Y) = 8 \quad \forall \lambda \in \mathbb{C} \text{ with } \text{Re}(\lambda) \geq 0. \tag{33}$$

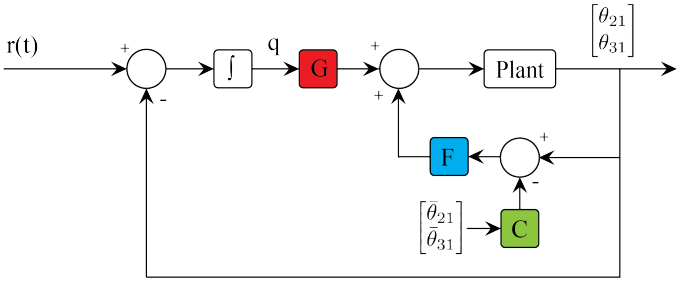

Fig. 2. Controller interaction with nonlinear plant

Because Q_z is a diagonal positive definite matrix, $Q_z^{1/2}$ is simply calculated by taking the square root of the diagonal elements.

$$Q_z^{1/2} = \text{diag}(\sqrt{a_1}, \sqrt{a_2}, \sqrt{b_1}, \sqrt{b_3}). \tag{34}$$

For the unstable eigenvalues $\lambda = 0$ of A_z, the matrix Y will always be full rank because rank$(-A_z) = 4$ and rank$(Q_z^{1/2}) = 4$. therefore $(A_z, Q_z^{1/2})$ is detectable and condition (iii) is met.

We have proved that all three conditions are met, thus it is guaranteed that there exists a unique positive definite solution P_z to the augmented ARE for any choice of positive definite R and positive semi-definite Q_z. The feedback law, which minimizes (26), is then given by

$$u = -R^{-1}B_z^\top P_z z \tag{35}$$
$$= F\delta\theta + Gq, \tag{36}$$

with gain matrices F and G defined as follows:

$$F := -R^{-1}B^\top P_{11}, \tag{37}$$
$$G := -R^{-1}B^\top P_{12}, \tag{38}$$

where $P_{11} \in \mathbb{R}^{2\times 2}$ and $P_{12} \in R^{2\times 2}$ are the matrices found through partitioning P_z as

$$P_z = \begin{bmatrix} P_{11} & P_{12} \\ P_{12}^\top & P_{22} \end{bmatrix}.$$

The closed-loop state-space representation of the linearized system model is given by

$$\dot{z} = \begin{bmatrix} A + BF & BG \\ -C & 0 \end{bmatrix} z + B_r r, \tag{39}$$
$$y = C_z z. \tag{40}$$

For the nonlinear system model, the feedback control law is the same, but the measured state is now θ instead of $\delta\theta$. It is of note that the feedback control law for the nonlinear system is no longer optimal. The block diagram of the resulting control system is provided in Fig. 2 where the nonlinear "Plant" is defined by (7).

C. Weight Matrix Selection and Tuning

The weight matrices Q_z and R were designed through an iterative tuning process which was guided by two key performance objectives:

1) Over/undershoot $< 5\%$ from reference values, and
2) rise time of less than 300 ms for tracking phase angle references.

Large weights on the integrator states in Q_i emphasize tracking accuracy over minimizing control effort, while smaller weights in R prevent large control actuation while maintaining responsiveness. Phase state weights in Q_θ have minimal impact on transient performance and can be normalized to 1. This weighting strategy achieves design goals without using complicated optimization frameworks.

IV. Simulation Results

For all numerical experiments, we set the system parameters to the values collected in Table 1. Following the weight matrix selection and tuning procedure in Section III-C, we have determined that

$$Q_z = \text{diag}\left(1, 1, \frac{0.1}{m_p^4}, \frac{0.1}{m_p^4}\right), \tag{41}$$

$$R = \text{diag}(10, 10). \tag{42}$$

TABLE I
Parameter Values

Symbol	Description	Value	Unit
S_r	Rated inverter power	4000	VA
V°	Nominal voltage	100	V RMS
ω°	Nominal frequency	$2\pi \cdot 60$	rad/s
R_g	Grid-side filter resistance	0.28	Ω
X_g	Grid-side filter reactance	0.35	Ω
$\overline{Z}_g$	Grid-side filter impedance	0.28+j0.35	Ω
$\lvert\overline{Z}_{loop}\rvert$	Δ-loop impedance magnitude	1.355	Ω
ϕ	Angle of Δ-loop impedance	0.896	rad
K	Constant in (7)	5.796	V
$\Delta\omega_{max}$	Max frequency deviation	$2\pi 0.5$	rad/s
ΔV_{max}	Max voltage deviation	$0.05V^\circ$	V
m_p	Real power droop slope	7.854×10^{-4}	V/W
m_q	Max voltage deviation	1.25×10^{-3}	rad/(sVar)

A. Linearized System Behaviour under LQI Control

The LQI controller's performance was first validated on the linearized closed loop system (39), starting at the equilibrium initial condition $z = \begin{bmatrix}0 & 0 & 0 & 0\end{bmatrix}^\top$. A step reference $r = \begin{bmatrix}15^\circ & -15^\circ\end{bmatrix}^\top$ was applied at time $t = 0$ s to observe the transient response of the closed-loop system. This reference was chosen because the maximum phase deviation (30° for this set of references) is above the typical fault detection threshold of 25° for IBR systems [12]. A fault would be detected by the system's protection relays, triggering appropriate protective actions according to grid code requirements. As shown in Fig. 3, the controller achieves rapid tracking with rise times of 202 ms and 287 ms for $\delta\theta_{21}$ and $\delta\theta_{31}$ respectively, minimal overshoot (3.6% for $\delta\theta_{21}$ and 0.16% for $\delta\theta_{31}$), and zero steady state error. The control signals settle quickly and smoothly, confirming robust performance.

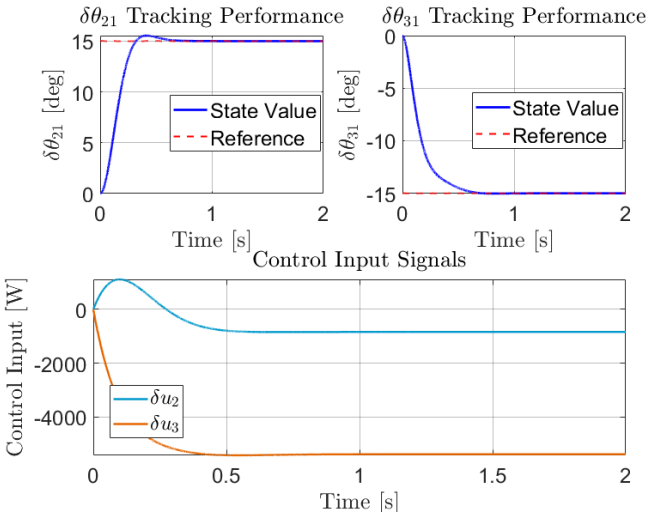

Fig. 3. Linearized system response to a step reference, demonstrating fast tracking and minimal overshoot

B. Nonlinear System Behaviour under LQI Control

Having established promising controller performance on the linearized system model, we assessed its robustness on the full nonlinear system model given in (9)- (11), where the inputs u_2 and u_3 were defined by the feedback law (36), and the reference is chosen as follows. From $t = 0$ to $t = 1$ s, the reference is set to be the phase-balanced equilibrium. At $t = 1$ s, the reference changes to follow

$$r(t) = \begin{cases} \begin{bmatrix}\bar{\theta}_{21} & \bar{\theta}_{31}\end{bmatrix}^\top & 0 \le t < 1 \text{ s}, \\ \begin{bmatrix}\bar{\theta}_{21} + 15^\circ & \bar{\theta}_{31} - 15^\circ\end{bmatrix}^\top & t \ge 1 \text{ s}. \end{cases} \tag{43}$$

Figure 4 illustrates that the LQI controller regulates the nonlinear system to the desired reference, with rise times of 285 ms for θ_{21} and 270 ms for θ_{31}, and close to zero overshoot. The control signals shown in Fig. 5 resemble those of the linearized system (Fig. 3), as expected given the assumption $\delta u_2 = u_2$ and $\delta u_3 = u_3$ due to $u_1 = 0$. The control signals generated by the LQI controller seen in Fig.5 show a similar time-domain response to the linearized system reference tracking test, which is expected due to the relationship $\delta u_2 = u_2$ and $\delta u_3 = u_3$ from the assumption that $u_1 = 0$ for all time.

The frequency of each inverter was extracted by back-calculating $\dot{\theta}_1, \dot{\theta}_2$, and $\dot{\theta}_3$ using (7). As seen in Fig. 6, when the reference is set to be the phase-balanced equilibrium, all three inverters have the same frequency equal to 60 Hz. When the reference changes at $t = 1$ s, the frequencies of each inverter go through their own transients and eventually settle to around 59.724 Hz in approximately 700 ms. The maximum frequency deviation, defined as the difference between the highest and

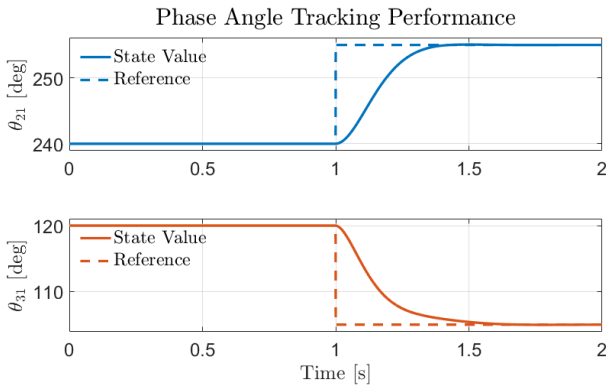

Fig. 4. Nonlinear system response to a changing reference, displaying fast tracking and favorable transient performance

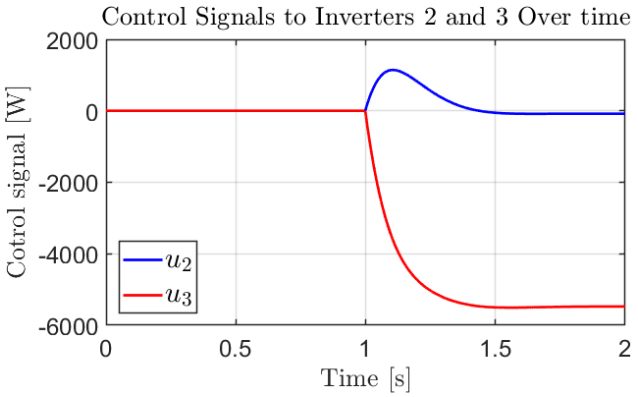

Fig. 5. Control inputs for the nonlinear system, consistent with linearized case

lowest frequencies observed among the inverters during a specified time interval, can be controlled through adjustments to the R matrix. Higher weights in the R matrix directly correlate with reduced maximum frequency deviations, enabling precise control of the inverter's output frequency during intentional phase unbalancing.

V. Concluding Remarks

In this paper, we presented a phase difference-based LQI control for single-phase grid forming inverters arranged in a delta configuration. The proposed LQI controller shows robust phase angle regulation, supporting unbalanced operation for improved fault injection and balancing of phases for nominal conditions. Simulation results confirm the controller's effectiveness under both nominal and simulated faulted conditions for the linearized and nonlinear system model.

Future work will involve experimental validation on hardware-in-the-loop (HIL) testing and applications to microgrid systems, highlighting the potential of this approach for enhancing protection and reliability in inverter-dominated grids. Further research includes conducting sequence analysis of the system and developing a controller that maps phase differences to sequence components for targeted fault injection and detection.

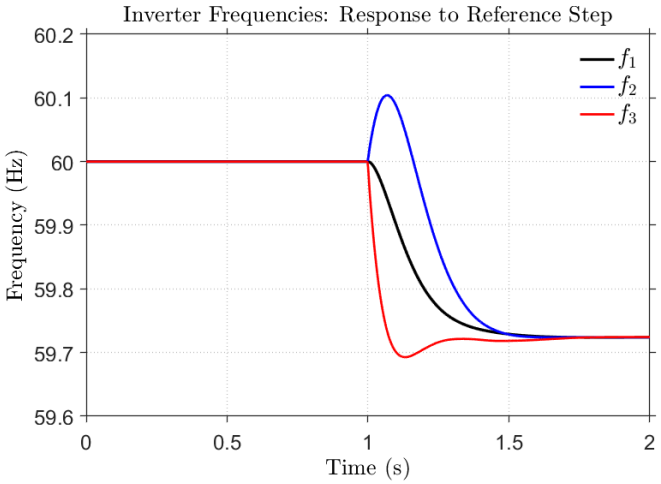

Fig. 6. Calculated frequency of each inverter over time due to a reference step at $t = 1s$

References

[1] A. Hooshyar and R. Iravani, "Microgrid protection," *Proceedings of the IEEE*, vol. 105, no. 7, pp. 1332–1353, 2017.

[2] N. Baeckeland, D. Chatterjee, M. Lu, B. Johnson, and G.-S. Seo, "Overcurrent limiting in grid-forming inverters: A comprehensive review and discussion," *IEEE Transactions on Power Electronics*, vol. 39, no. 11, pp. 14 493–14 517, 2024.

[3] J. A. Taylor and A. D. Domínguez-García, "Active fault detection in static systems," *IEEE Transactions on Automatic Control*, pp. 1–8, 2025.

[4] A. Banaiemoqadam, A. Hooshyar, and M. A. Azzouz, "A comprehensive dual current control scheme for inverter-based resources to enable correct operation of protective relays," *IEEE Transactions on Power Delivery*, vol. 36, no. 5, pp. 2715–2729, 2021.

[5] T. Qoria, H. Wu, X. Wang, and I. Colak, "Variable virtual impedance-based overcurrent protection for grid-forming inverters: Small-signal, large-signal analysis and improvement," *IEEE Transactions on Smart Grid*, vol. 14, no. 5, pp. 3324–3336, 2023.

[6] J. A. Taylor and A. D. Domínguez-García, "Auxiliary signal-based distance protection in inverter-dominated power systems," in *Proceedings of the European Control Conference (ECC)*, Stockholm, Sweden, Jun. 2024. [Online]. Available: https://paperhost.org/proceedings/controls/ECC24/files/0369.pdf

[7] O. Ajala, M. Lu, B. Johnson, S. V. Dhople, and A. Domínguez-García, "Model reduction for inverters with current limiting and dispatchable virtual oscillator control," *IEEE Transactions on Energy Conversion*, vol. 37, no. 4, pp. 2250–2259, 2022.

[8] W. Cai, R. Mallik, and B. Johnson, "Singular-perturbation-based control design of single-phase grid-forming inverters," in *2024 IEEE Energy Conversion Congress and Exposition (ECCE)*, 2024, pp. 893–900.

[9] M. Lu, S. Dhople, D. Zimmanck, and B. Johnson, "Spontaneous phase balancing in delta-connected single-phase droop-controlled inverters," *IEEE Transactions on Power Electronics*, vol. 37, no. 12, pp. 14 115–14 125, 2022.

[10] P. C. Young and J. C. Willems, "An approach to the linear multivariable servomechanism problem," *International Journal of Control*, vol. 15, no. 5, pp. 961–979, May 1972.

[11] T. Basar, S. Meyn, and W. R. Perkins, "Lecture notes on control system theory and design," 2024, [Online]. Available: https://arxiv.org/abs/2007.01367. [Online]. Available: https://arxiv.org/abs/2007.01367

[12] *IEEE Standard for the Interconnection and Interoperability of Inverter-Based Resources (IBRs) with Associated Electric Power Systems Interfaces*, IEEE Std., 2022, clause 7.3.2.4. [Online]. Available: https://standards.ieee.org/standard/2800-2022.html